Exploring strength and ductility responses of beam-column joints composed UHPC and UHPFRC employing concrete damaged plasticity

Guilherme Santos da Silveira, Carlos Natã Zenatti, Gustavo de Miranda Saleme Gidrão, Rúbia Mara Bosse, Paulo Rogério Novak
Federal University Technology of Paraná - UTFPR, Brazil
gsilveira_s@outlook.com.br, http://orcid.org/0000-0001-2345-6789
carlosnzenatti@gmail.com, https://orcid.org/0009-0002-8067-8614
gustavo.gidrao@gmail.com, https://orcid.org/0000-0003-1483-0526
rubiambosse@utfpr.edu.br, https://orcid.org/0000-0003-4153-3455
novak@utfpr.edu.br, https://orcid.org/0000-0003-3080-8564

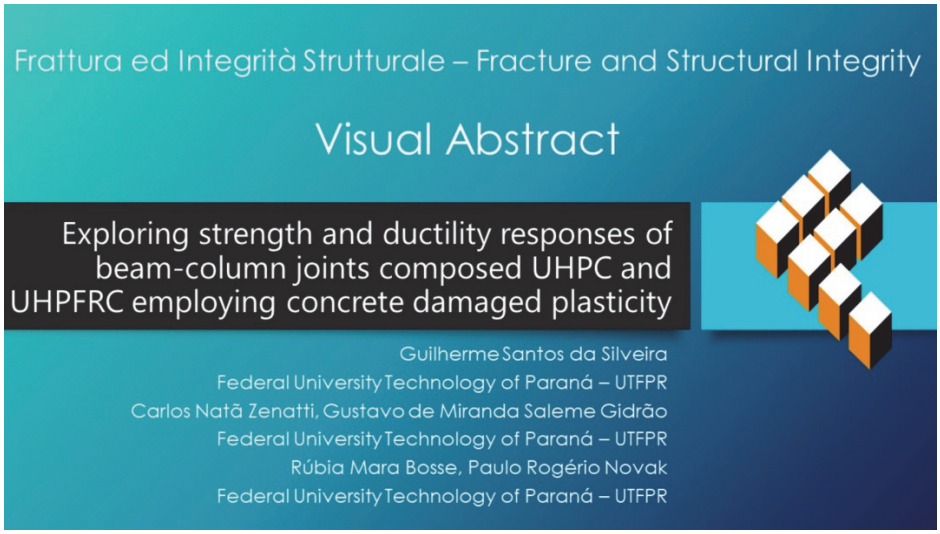

Citation: Silveira, G. S., Zenatti, C. N., Gidrão, G. M. S., Bosse, R. M., Novak, P. R., Exploring strength and ductility responses of beam-column joints composed UHPC and UHPFRC employing concrete damaged plasticity, Frattura ed Integrità Strutturale, 68 (2024) 77-93.

Received: 17.10.2023
Accepted: 04.01.2024
Published: 18.01.2024
Issue: 04.2024

KEYWORDS. Beam-column joints, UHPFRC, CDP, Ductility, Failure.

INTRODUCTION

Beam-column joints represent discontinuous regions characterized by abrupt changes in geometry or material properties. The presence of construction defects in these joints, often due to the density and arrangement of reinforcements, can amplify the critical nature of these regions. Such areas are prone to nonlinear behavior, particularly under substantial loads or during events that exert significant lateral forces on structures, such as windstorms or earthquakes. This nonlinear behavior accentuates the criticality of beam-column joints, rendering them more vulnerable to failure than other structural components. A failure at these connections can lead to a chain reaction of failures throughout

the structure, potentially leading to a collapse. Hence, a rigorous design and comprehensive understanding of beam-column joints are essential for ensuring structural safety. The intrinsic complexity of these elements, arising from nonlinearity and discontinuities, highlights their pivotal role in preserving the safety and stability of the entire structure [1-3].

Localized cracking patterns withing beam-column joints can be indicative of the formation of structural hinges across the system. Such hinges can compromise the integrity of the structure, especially when subjected to dynamics loads. When these patterns emerge, it becomes crucial for the structure to possess the inherent capability to redistribute loads. This redistribution ensures that stress concentrations are alleviated, channeling internal forces to adjacent, undamaged joints.

The emergence of localized cracking, often suggestive of an inelastic hinge, can precipitate a potential collapse mechanism within the framing system, as represented by failures modes: soft-story, local and global mechanisms. Local and soft-story failures often occur in highly ductile structures, leading to element collapse. Conversely, the global failure mechanism gradually collapses as the structure dissipates energy from actions with lower structural ductility demands. Thus, this failure mode takes precedence in seismic and dynamic scenarios [2-4]. It is worth noting that collapse mechanisms (e.g., soft-story) are more critical regarding structural reliability. They typically involve a limited number of compromised elements, challenging their detection and mitigation. Moreover, their manifestation often signals a brittle, rather than ductile, failure mode, which can be catastrophic if not addressed promptly [2-5].

Costa et al. [6] examined the dynamic behavior of beam-column joints constructed with regular-strength concrete under seismic conditions in their study. Their findings revealed significant damage within these joints, indicating notably high average tensile damage values (d_t) exceeding 0.79. This highlights the structural vulnerability of the building, indicating a potential risk of overall collapse due to increased bending moments and shear forces at these critical connections.

According to Taranath [7], when exposed to seismic tremors, reinforced concrete structures need to endure a spectrum of earthquakes. From mild tremors causing no damage to moderate ones resulting in minimal structural damage and some non-structural impact, these structures, even in severe earthquakes, may sustain structural and non-structural damage without collapsing.

A study explored the key factors significantly impacting structural stability, particularly concerning the capacity of beam-column joints. These include the prior axial load on the column, the geometric relationship between the beam and column, the concrete's compressive strength, the distribution of steel bars, the type of reinforcement, the reinforcement ratios, and the crack width [8-12]. In this context, Kim and LaFave's [13] study, conducted across various parameters, underscored the preeminent role of concrete strength in shaping critical outcomes. The strength of concretes above 110 MPa is limited, in database of Chetchotisak et al. [9] with 328 tests. This emphasizes the predominant research focus on medium-strength concrete at 40 MPa (70.7%), with an increasing emphasis on high-strength concrete at 60 MPa (16.8%) and ultra-high-strength at 110 MPa (12.5%).

In addressing the critical zones of beam-column joints, both Ultra-High-Performance Concrete (UHPC) and its fiber-enhanced variant, Ultra-High-Performance Fiber-Reinforced Concrete (UHPFRC), stand out as optimal materials. They boast great compressive and tensile capacities. Their intrinsic ductility is particularly crucial in seismically active areas, facilitating efficient energy absorption and mitigation. UHPC's compact microstructure offers superior resilience against environmental factors, and the embedded fibers in UHPFRC provide a robust defence against crack evolution, safeguarding the integrity of the connection. With their exceptional adhesion properties and the versatility, they bring to structural design, these advanced concretes not only ensure superior structural behavior but also promise cost-effectiveness over the long term, positioning them at the forefront of contemporary construction research and practice [14-18].

In the field of structural engineering, computational simulations have emerged as an indispensable tool. When analyzing beam-column joints, which are crucial for the stability and performance of structures, these simulations enable the evaluation of various connection designs and loading scenarios. Particularly when examining advanced materials like UHPC and UHPFRC, for which mechanical models and constitutive laws have already been validated in the literature, computational simulations provide a cost-effective and efficient approach to predicting and analyzing structural behaviors. By leveraging these simulations, researchers and engineers can refine joint designs, foresee potential challenges, and ensuring safety for the structures [19-21].

Consequently, this research delves into the impact on ductility and strength of a beam-column joint composed of Ultra-High-Performance Concrete (UHPC) and UHPFRC. The numeric simulation is supported by the expansion of the numerical-experimental model crafted from Low-Strength Concrete (LSC) as formulated by Cosgun et al. [22] and subsequently numerically simulated by Abdelwahed et al. [23].

The nonlinear behavior of concrete can be effectively represented by the Concrete Damaged Plasticity (CDP) model developed by Lubliner et al. [24] and Lee and Fenves [25], catering to both static and dynamic loadings in low cycles. However, addressing structural fatigue in high cycles presents challenges due to the difficulty in capturing damage through independent variables and the absence of necessary parameters to represent the heterogeneous behavior of materials under

high cycles and multiaxial loadings [26-27]. For high-cycle analysis, using more robust models, such as the CDPM2 model by Grassl et al. [28] and the Enhanced Damage Plasticity (ECDP) proposed by Kakavand and Taciroglu [29], is essential. In this manner, the present study applies the CDP model to represent the behavior of portal joints under the studied static loading. The results indicate that UHPFRC joints exhibit superior strength, enhanced ductility, and a distinctive damage progression pattern.

CONCRETE DAMAGED PLASTICITY (CDP)

The elastoplastic damage model captures the intricate nonlinear features of materials, encompassing the gradual accumulation of deformations and subsequent degradation of the elastic modulus under monotonic loading. The Concrete Damaged Plasticity (CDP) model stands out for its ability to represent both elastic and plastic damage accumulation, leading to material stiffness reduction. This effect is applied to the Cauchy stress tensor to describe behavior under compression (σ_c) and tension (σ_t) (Eqs. 1 and 2). This model characterizes uniaxial stress-strain behavior, delineating plastic ($\varepsilon_{c,pl}$) and elastic ($\varepsilon_{c,pel}$) deformations in both phases (compression and tension), culminating in the total strain (ε), represented by the sum of these components [30-32]. This model is founded on elasticity theory and encompasses the concrete failure criteria of the Drucker-Prager model (k_c), limited to 3D solid models [33].
The provided text describes the Figs. 1 and 2 presenting concrete's uniaxial compressive and tensile responses using the CDP, considering the degree of damage under compression (d_c) and tension (d_t) associated with the reduction in stiffness due to the initial modulus of elasticity (E_0) [34].

$$\sigma_c = \left(\frac{1-d_c}{\varepsilon-\varepsilon_{pl}}\right)E_0 = \frac{E_{el}}{\varepsilon-\varepsilon_{pl}} \tag{1}$$

$$\sigma_t = \left(\frac{1-d_t}{\varepsilon-\varepsilon_{pl}}\right)E_0 = \frac{E_{el}}{\varepsilon-\varepsilon_{pl}} \tag{2}$$

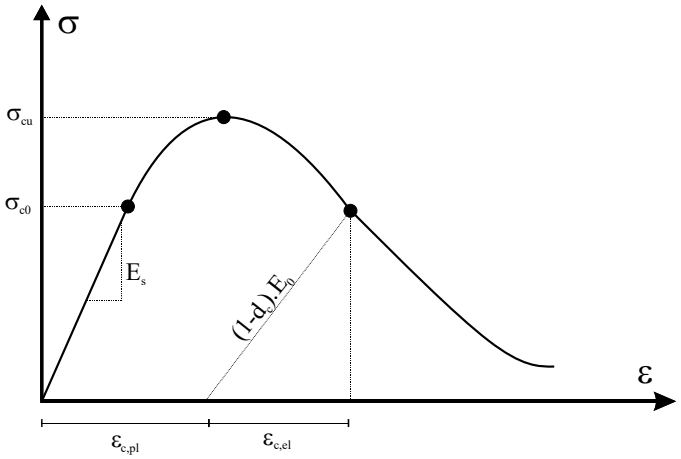

Figure 1: Uniaxial compression stress-strain [35].

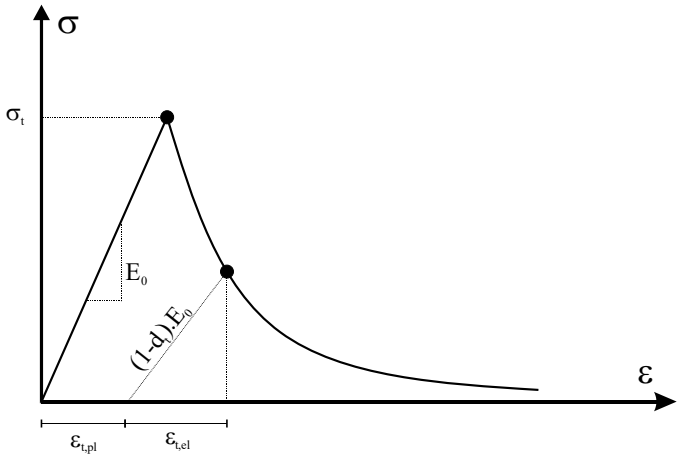

Figure 2: Uniaxial tensile stress-strain [35].

To perform numerical modelling, it is necessary to input the material's elasticity parameters, such as Young's modulus and Poisson's ratio. These parameters define the elastic properties of the material and initiate the analysis of the plasticity variables within the Concrete Damaged Plasticity. Incorporating the stress-strain and damage-strain relationships allows the nonlinear behaviour and damage evolution within the structure to be captured. These relationships accurately describe how material properties evolve as plastic deformations and damage accuracy and it is the specific CDP parameters: ψ is the dilation angle of the solid, *m* an eccentricity, σ_{b0}/σ_{c0} the tension biaxial behaviour failure ratio, k_c is defining the failure surface in the deviatoric plane normal to the solid's hydrostatic axis and ν a virtual-numerical viscosity of the solid. These parameters are represented in Tab. 1.

Concrete	ψ	m	σ_{b0}/σ_{c0}	k_c	v
LSC [23]	45°	0.1	1.07	0.666	0.0002
NSC	45°				0.0001
UHPC [36]	50°				
UHPFRC [36]	55°				

Table 1: Parameters of CDP input the model on Abaqus.

DUCTILITY INDEXES

Ductility measures the ability of an element to withstand plastic deformations before experiencing a fracture. Its representation is closely tied to the elastic and plastic behaviour, as illustrated by the stress-strain curve of materials [37]. Both ductility and strength are critically important properties for ensuring appropriate structural performance. Ensuring ductile failure is critical to enhancing safety [34]. The energy-based ductility index (μ_e), introduced by Naaman and Jeong [38], is calculated by applying the approach illustrated in Fig. 3, following Eq. 3, until the ultimate force (P_u) is reached.

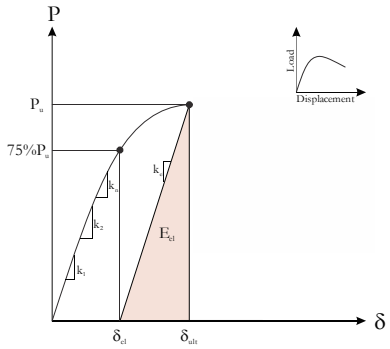

Figure 3: Energetic ductility [39].

$$\mu_e = \frac{1}{2}\left(1 + \frac{E_{total}}{E_{elastic}}\right) \tag{3}$$

The energy calculation involves integrating the graph shown in Fig. 3, where the elastic energy (i.e., $E_{elastic}$) describes the material's behavior up to the elastic limit, and the total energy (E_{total}) encompasses the displacement up to the ultimate deformation (δ_{ult}) of the solid.

The energy-based index (μ_e) offers an advantage due to its formulation inherently considering concrete's elastic-plastic behavior, depicting the extent of material deformation before fracturing [34, 40]. Thus, it allows for assessing a structure's ductility and comprehension of its performance concerning concrete strength properties. According to AFGC [41] and NF P18-710 [42], structures made of UHPFRC should exhibit sufficient ductility post-failure, ensuring that the tensile stress at rupture exceeds 3 MPa. These aspects can be linked to critical factors, ensuring enhanced user safety. Typically, higher ductility indices indicate that failure initiates with reinforcement yielding, with stresses absorbed by the concrete's deformation until eventual failure due to concrete crushing [42].

NUMERICAL MODELING

Thus, this study employs computational analysis via the finite element method in Abaqus software. It builds upon a simplified damage assessment from CDP, expanding the study of Cosgun et al. [22] to the UHPC. A significant contribution of this study is the understanding of the behavior of beam-column joints made of UHPC, UHPFRC,

usual and low-strength concrete (LSC), with an emphasis on the ductile response of each design. This enhancement is achieved by incorporating UHPC or UHPFRC, resulting in improved and more robust structural behaviour.
The analysis focuses on an end-node of a frame subject to monotonic loading conditions with stirrups spaced at intervals of 50 mm and 100 mm, as per the detailing in Fig. 4 for the beam and column. Initially a numerical calibration based on Cosgun et al. [22] , followed by the calibration conducted by Abdelwahed et al. [23]. Subsequently, a parametric numerical analysis was extended to evaluate the performance of UHPC and UHPFRC, explicitly focusing on assessing strength and ductility. Fig. 5 displays the boundary conditions in the example conducted by Cosgun et al. [22].
The simulation proceeded through two sequential stages: (1) at point P1, this application of a static axial the 20 kN (Step-1); (2) the application of a vertical displacement of 60 mm at the beam in point P2 (Step-2), as illustrated in Fig. 5.

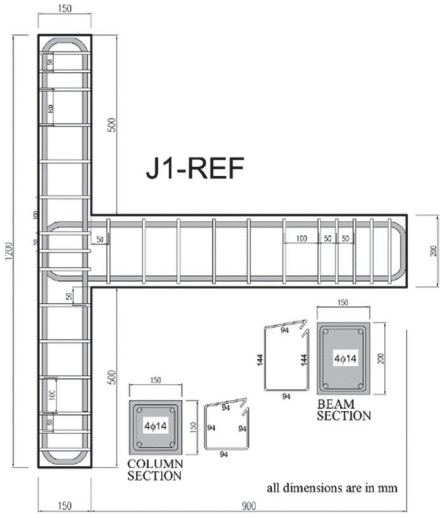

Figure 4: Experimental model beam-column [22].

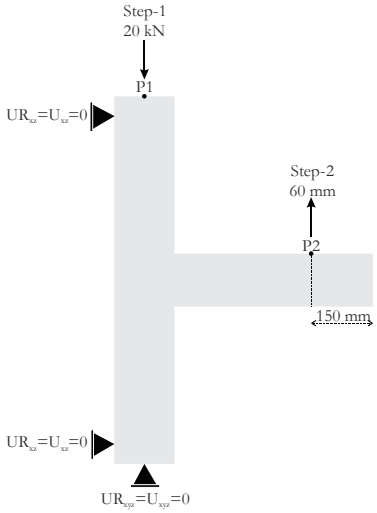

Figure 5: Model boundary conditions.

Geometry and elements types

Figs. 6 and 7 show the structural modelling. The concrete components are represented by solid elements with 8 nodes each and reduced integration (C3D8R), while the steel reinforcements are represented by 3D truss elements with 2 nodes each (T3D2). The reinforcement bars are considered to adhere perfectly to the surrounding concrete, characterized as an 'embedded region' interface property [6, 23, 34].

Figure 6: Concrete.

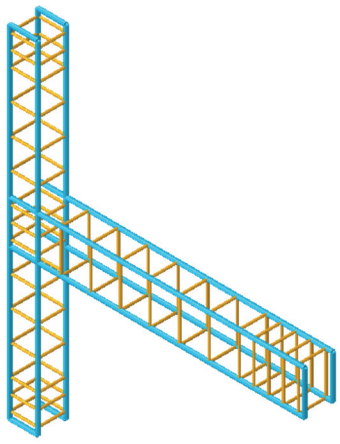

Figure 7: Reinforcement of concrete.

Constitutive law of materials

Cosgun et al. [22] and Abdelwahed et al. [23] adopted the assumption of perfect plasticity to model the behavior of the reinforcement elements (Tab. 2). For the concrete, CDP was applied to represent the nonlinear response of the material.

Reinforcement	Diameter's bars	Poisson's ratio	Modulus of elasticity	Plastic strain	Yield stress
Longitudinal	14 mm	0.30	200 GPa	0	445 MPa
				0.021	625 MPa
Stirrups	8 mm			0	276 MPa
				0.013	420 MPa

Table 2: Parameters of steel input the model on Abaqus [23].

To characterize the LSC, we applied the constitutive laws outlined in Figs. 8 and 9, formulated by Abdelwahed et al. [23], to Cosgun et al.'s experiment [22].

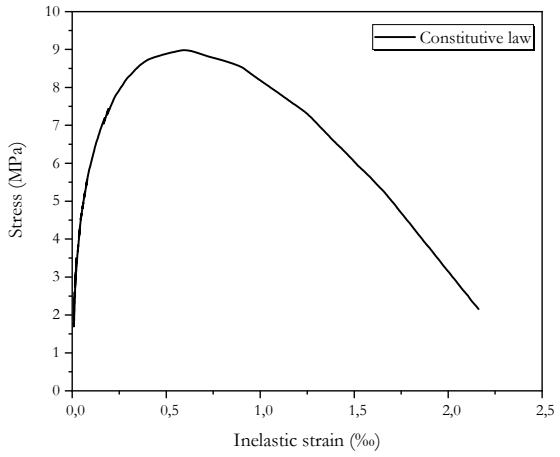

Figure 8: Compressive behavior under the CDP [23].

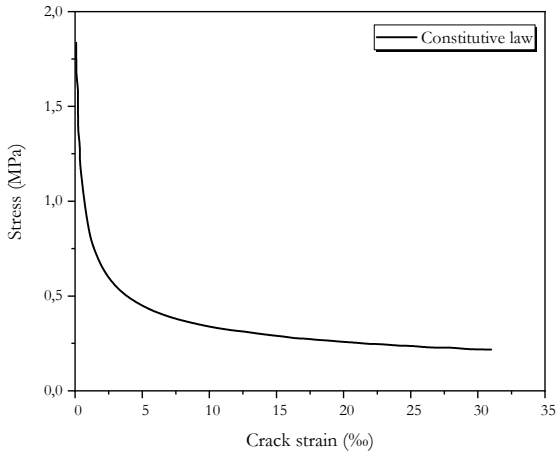

Figure 9: Tensile behavior under the CDP [23].

The elastic modulus of the LSC is determined through the empirical formulation by Ahmad et al. [44], with Eq. 4 describing the property for low-strength concretes. The calibration parameters utilize ACI 318 [45], EC2 [46], and CEB FIP Model Code [47] guidelines, which provide analytical representations. Furthermore, Kumar [47] and Sima et al. [48] conducted experimental studies on this property for concrete classes with strengths ranging from 5 MPa to 15 MPa.

$$E_c = 17081\left(\frac{f_{ck}}{10}\right)^{0,42} \tag{4}$$

In the numerical simulations performed to investigate the use of NSC, UHPC and UHPFRC at the joint model, we employed the inelastic response compressive behavior developed by Carreira and Chu [50] (Fig. 10). Additionally, the tensile stress-inelastic strain formulation developed by Krahl et al. [36] was used to characterize the tensile response of UHPFRC, while the methodology outlined in the CEB FIP Model Code [47] was adopted to describe the tensile behavior of NSC and UHPC (Fig. 11). Finally, Tab. 3 presents the input parameters for simulation and calibration:
The CDP governed by progressive damage accumulation, as described in the simplified model's compression (Eq. 5) and tensile response (Eq. 6).

$$d_c = 1 - \frac{f_c}{\sigma_c} \tag{5}$$

$$d_t = 1 - \frac{f_t}{\sigma_t} \tag{6}$$

In this context, σ_t and σ_c denote the tension and compression stresses. Additionally, f_t and f_c are the stress levels associated with inelastic deformation. This simplification aids in explaining the progression of damage, which becomes evident after the concretes represents the accumulation of damage for the different concrete types under study in Figs. 12 and 13.

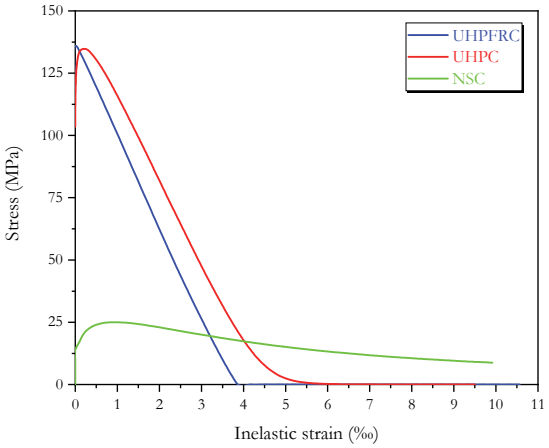

Figure 10: Inelastic stress-strain under uniaxial compression.

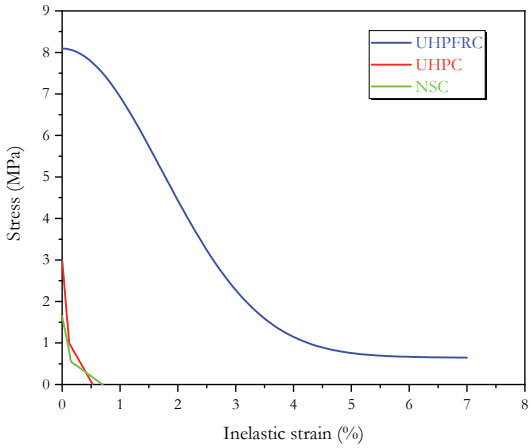

Figure 11: Inelastic stress-strain under uniaxial tension.

Concrete	Poisson's ratio	Modulus of elasticity	Compression stress	Tension stress
LSC [23]	0.20	17039 MPa	9 MPa	1.86 MPa
NSC		26064 MPa	25 MPa	1.65 MPa
UHPC [36]		45000 MPa	135 MPa	3.00 MPa
UHPFRC [36]		43000 MPa		8.00 MPa

Table 3: Parameters of concrete input the model on Abaqus.

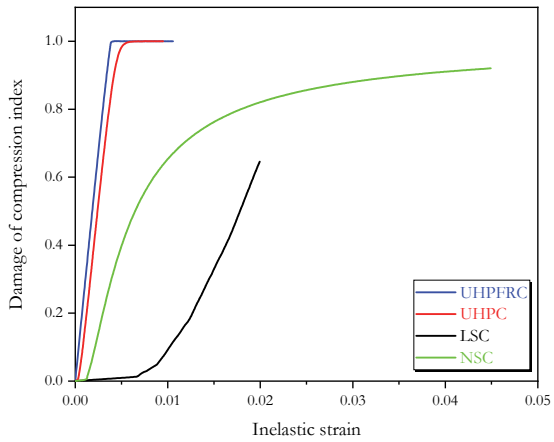

Figure 12: Damage of compression index.

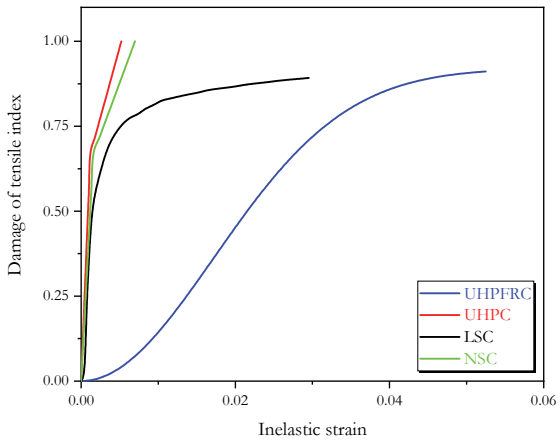

Figure 13: Damage of tensile index.

Analysis of mesh size convergence

The mesh selection process followed a thorough mesh convergence study to ensure comprehensive computational simulation. This study covered mesh convergence values ranging from 25 to 50 mm, and achieving convergence involved refining the numerical model related to the LSC element to align it with the experimental model conducted by Cosgun et al. [22]. The analysis accounted for the effective influence of Concrete Damaged Plasticity (CDP) behavior in Fig. 14 depicts the mesh convergence study considering the element's behavior without damage effects (i.e., plastic behavior). In Fig. 15,

the simplified damage was incorporated into the structural element as described in Eqs. 3 and 4. Both Figs. 14 and 15 illustrates the representation of the experimental response by Cosgun et al. [22] through a continuous black line.

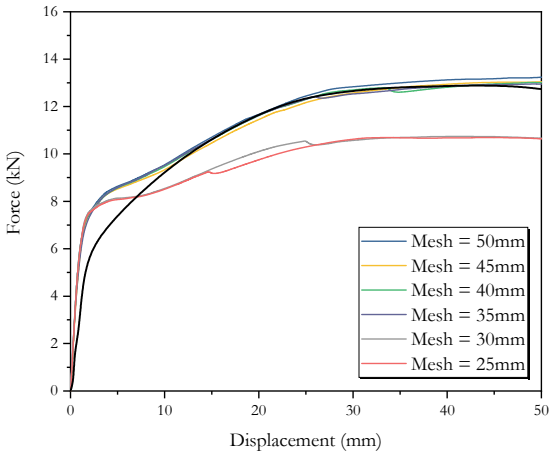

Figure 14: Mesh size with behavior plastic.

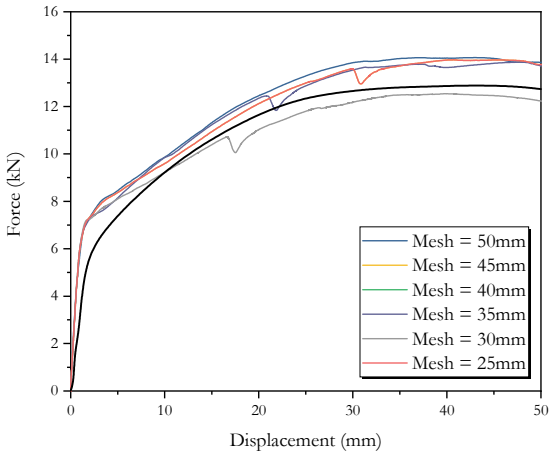

Figure 15: Mesh size with CDP.

The CDP model embodies the nonlinear behavior of concrete by reducing its mechanical properties, thereby associated with a decrease in material stiffness [6, 34]. Accordingly, the 35 mm mesh proves more efficient in describing concrete behavior while maintaining lower computational costs, as illustrated in Fig. 16. For this reason, this mesh size is adopted to represent the network of solid elements at the pillar node. For the reinforcements, a mesh spacing of 94 mm was used for longitudinal reinforcement and 14 mm for stirrups in the beams, and the columns' spacing was set at 99 mm and 9.4 mm, respectively.

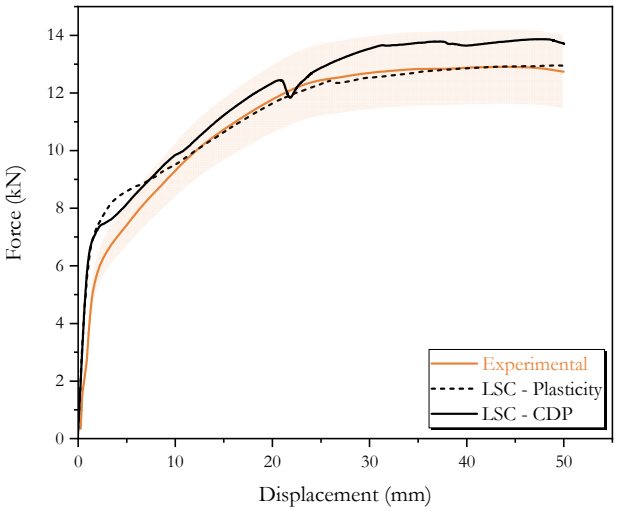

Figure 16: Validation of numerical simulation.

RESULTS

Numerical-experimental validation

The provided text discusses the outcomes of a computational simulation. It describes the application of static loading at point P1 and the vertical displacement at P2. Point P2 is utilized to analyze the numerical response and calibrate it with the experimental data from Cosgun et al. [22]. Fig. 16 illustrates the outcomes of the conducted computational simulation: the orange line shows the experimental result; the light orange area shows the experimental results with ±10%

error; the continuum black line shows the response of the CDP model, employing a simplified damage law (Eqs. 3 and 4); the dotted black line shows the response obtained with the perfect plasticity constitutive law. It can be noted that both simulations produce results accurate enough to represent the experimental one. Fig. 16 unveils that the calibrated model, derived from previous studies [22], demonstrates a disparity of less than 10% of the experimental force-displacement values for LSC, according to the orange area in the graph.

According to Brazilian Concrete Code - ABNT NBR 6118:2023 [51] structural design for the Ultimate Limit State (ULS) exhibits distinct stages of behavior, as illustrated in Fig. 17: (i) Stage 1 marks the commencement of loading with low-stress levels and linear distribution, ultimately leading to cracks in the structure; (ii) Stage 2 describes the concrete's maximum tensile strength, resulting in cracks in the tensioned section and a linear distribution in the compressed area. This phase holds significance in determining crack width and signifies the initiation of plasticization in the compressed concrete; and (iii) Stage 3 the concrete approaches the rupture point, attaining maximum tension and compression deformations.

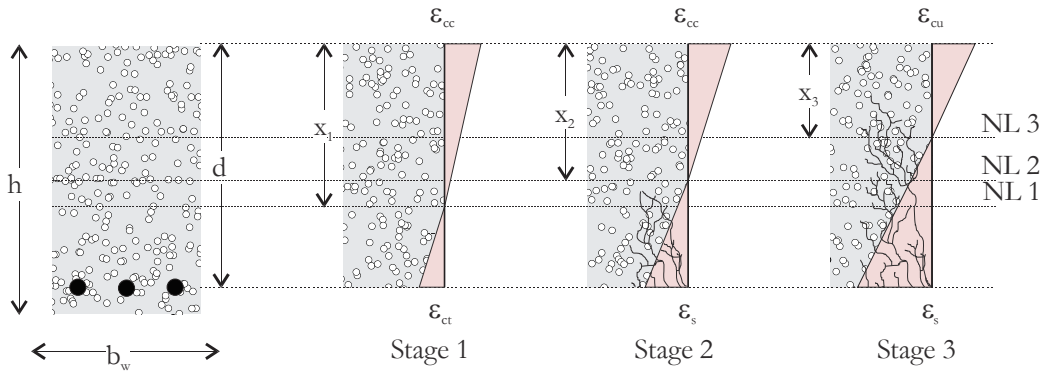

Figure 17: Stress-strain distribution in the ULS.

Simulation of joints with LSC, NSC, UHPC and UHPFRC

After the numerical validation, the study introduces the constitutive models for UHPC and UHPFRC (2.5% fiber volume, considered in the constitutive law) to be applied for structural assessment. Fig. 18 depicts the force-displacement curve for the joint previously modeled, constructed from LSC (represented in black), NSC (in green), UHPC (in red), and UHPFRC (in blue) along with their respective energetic ductility indices as shown in Fig. 3. The UHPFRC joint had the highest maximum load capacity of 41.44 kN, followed by 17.24 kN for the UHPC section, 15.66 kN for the NSC section, and 12.44 kN for the LSC section. These results indicate a significant increase in the relative strength of UHPFRC, UHPC, and NSC, with values of 3.33, 1.39, and 1.26 times, respectively, compared to the LSC section.

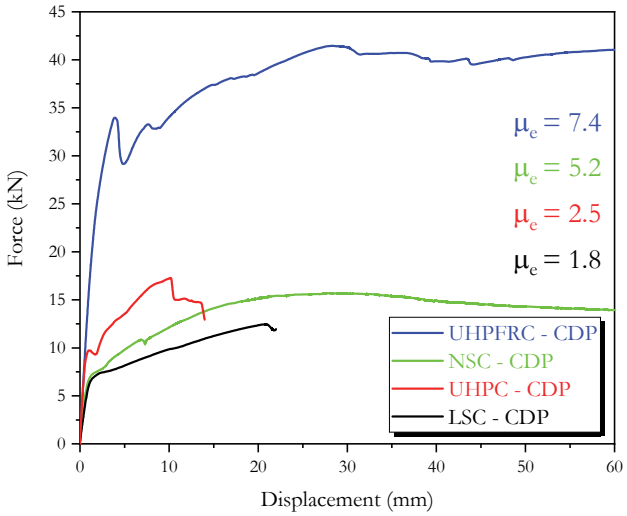

Figure 18: The energetic ductility indexes.

The energetic ductility index of UHPFRC is 4.11 times greater than that of LSC and 1.42 times greater than NSC. On the other hand, UHPC exhibited an energetic ductility index 1.39 times greater than LSC.

From Fig. 18 it can be observed that the presence of steel fibers in material indeed contributed to improve the ductile response of the UHPFRC joint. These steel fibers redistribute stress around the joint, increasing the load-carrying capacity and possibly change the cracking pattern observed. Figs. 19-22 show compression and tension damage maps, Von Mises Stress in concrete and Von Mises Stress in reinforcements at ultimate force for LSC, NSC, UHPC and UHPFRC joints respectively.

It can be noted from Fig. 22.b that UHPFRC joint showed a cracking pattern indicating flexural failure with vertical flexural damage evident. In Fig. 20.b (NSC joint) , the ultimate damage map indicates the formation of the strut-and-tie mechanism (STM) with failure possibly caused by bending moments. In contrast, in the cases of LSC and UHPC, as depicted in Figs. 19.b and 21.b, damage appears at discontinuous region, possibly indicating a brittle failure mode for the joint. This phenomenon is attributed to the increase in shear stress, leading to the formation of the STM, which is a consequence of the absence of fibers. Therefore, steel fibers play a crucial role in crack management. Particularly, in the case of UHPFRC, the higher Von Mises stress and distinct bending failure mode can be attributed to the steel fibers, enhancing the material's ductility and the efficiency of the steel bars. Therefore, steel fibers play a significant role in the observed failure modes of these joints [52-54].

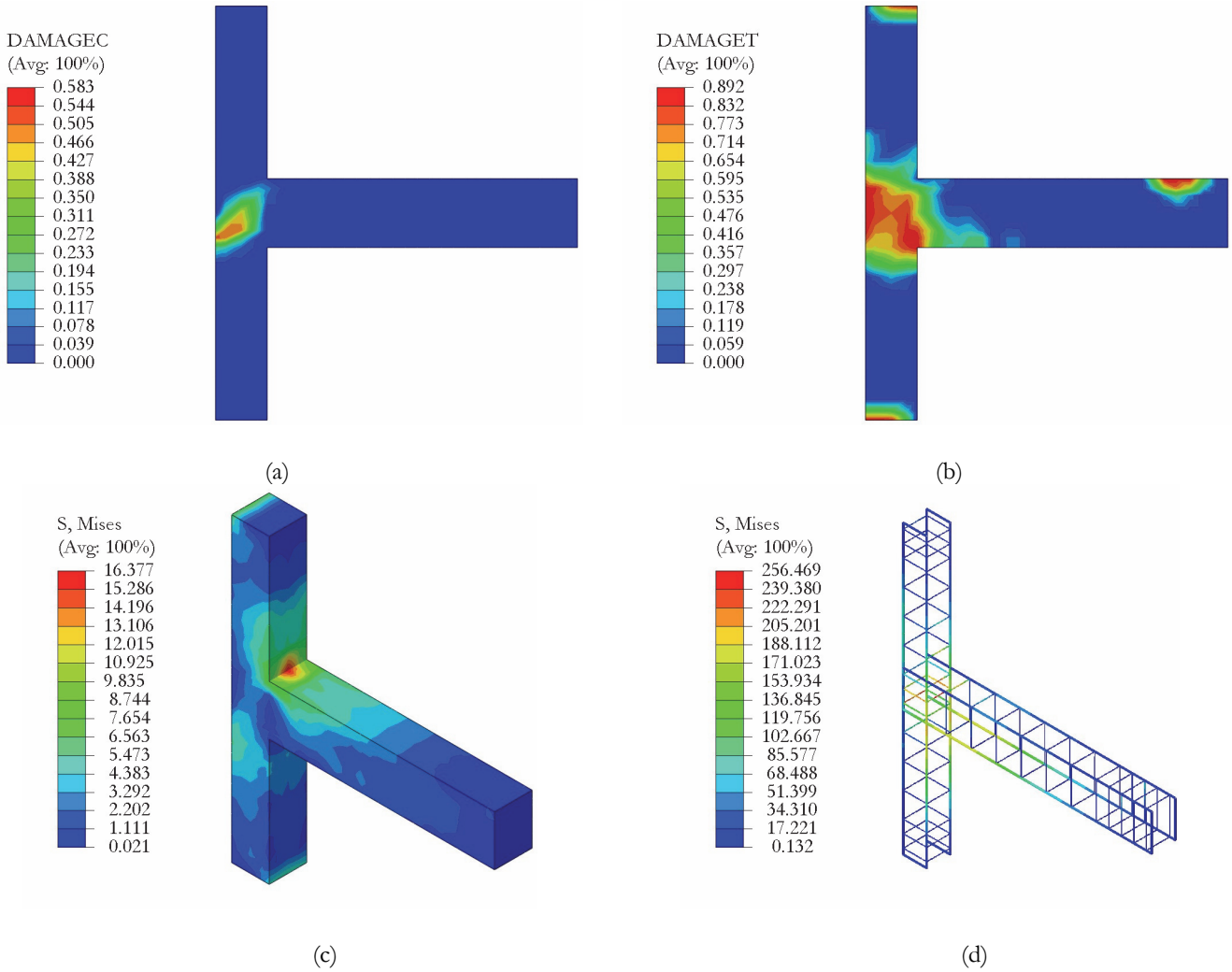

Figure 19: Simulation of LSC: (a) Damage in compression, (b) Damage in tension, (c) Von Mises Stress in concrete, and (d) Von Mises Stress in steel bars.

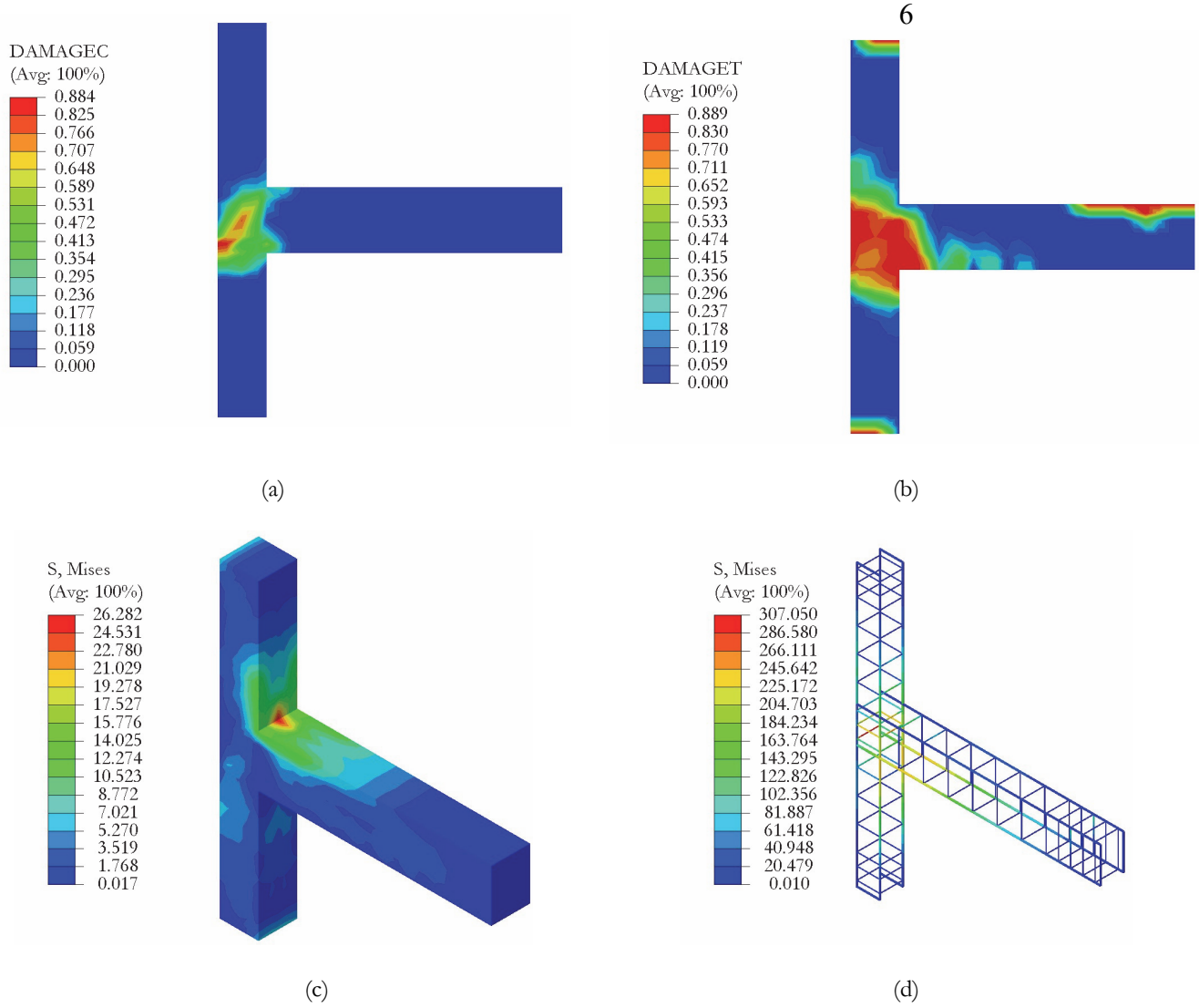

Figure 20: Simulation of NSC: (a) Damage in compression, (b) Damage in tension, (c) Von Mises Stress in concrete, and (d) Von Mises Stress in steel bars.

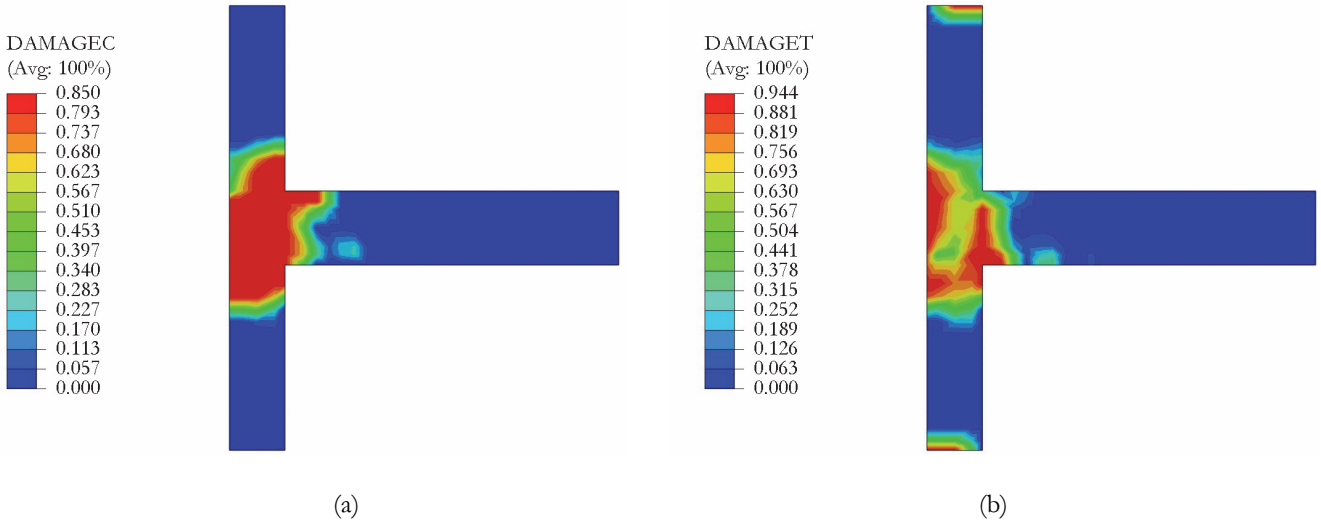

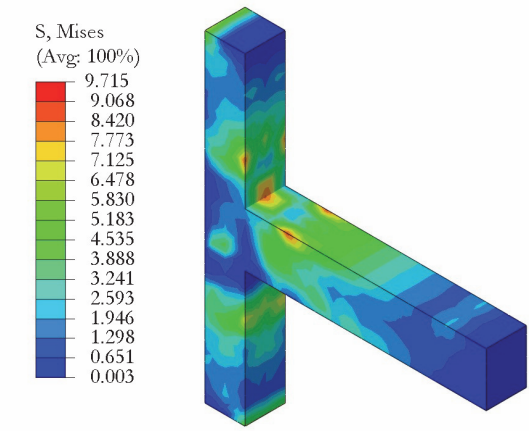

(c)

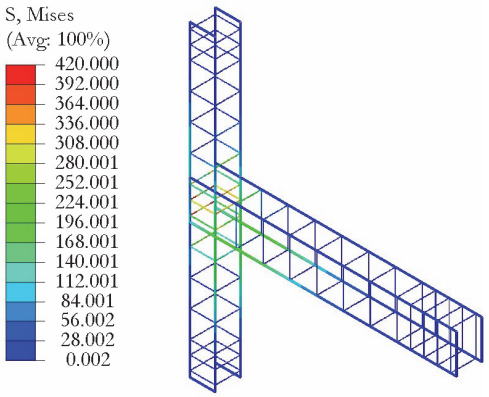

(d)

Figure 21: Simulation of UHPC: (a) Damage in compression, (b) Damage in tension, (c) Von Mises Stress in concrete, and (d) Von Mises Stress in steel bars.

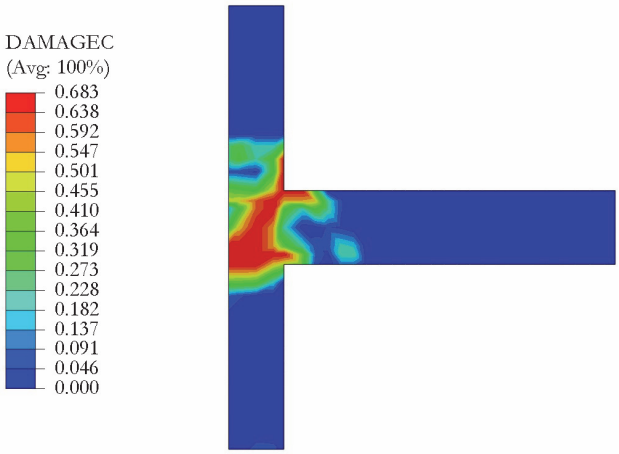

(a)

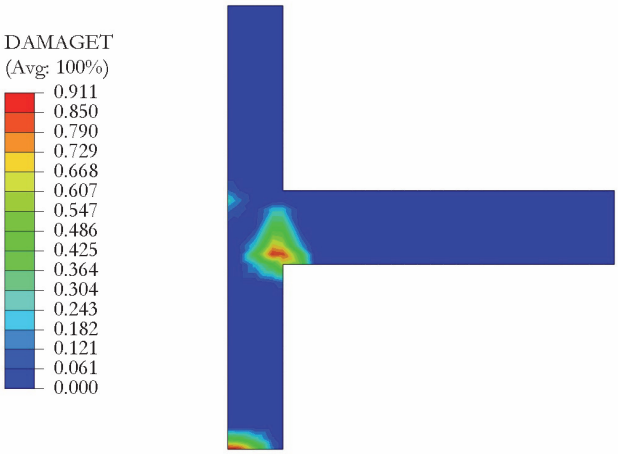

(b)

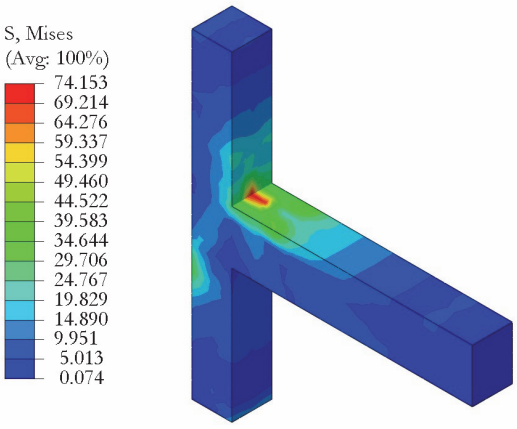

(c)

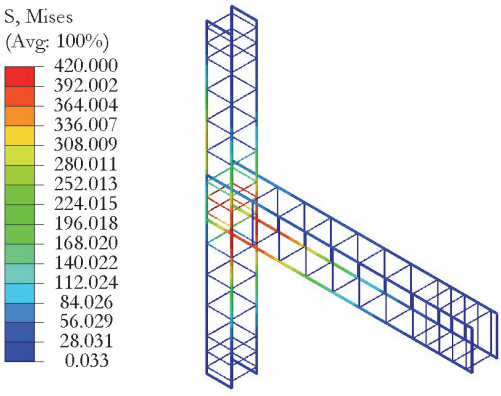

(d)

Figure 22: Simulation of UHPFRC: (a) Damage in compression, (b) Damage in tension, (c) Von Mises Stress in concrete, and (d) Von Mises Stress in steel bars.

The research on the behavior of frames, using various classes and types of concrete, plays a fundamental role in the analysis of the performance of these materials. In addition to enabling the evaluation of stresses and the rupture mechanism in structures, this approach also allows for a more in-depth analysis of reinforcements. This becomes evident when considering the information presented in Figs. 19-22. Remarkably, by employing UHPFRC we can largely maximize the stresses in the connection zone. This optimization, in turn, directly influences the damage pattern, as observed in the results obtained using UHPFRC.

In Fig. 23, a succinct overview of the critical parameters assessed in the study is presented. The Fig. 23.a highlights the capacity of UHPFRC to enhance the maximum forces resisted by the beam-column joints. Additionally, Fig. 23.b displays the force at which the model approaches the elastic limit, highlighting the superior performance of UHPFRC, particularly in terms of reaching service limit states, as the element progresses beyond stage 1 in Fig. 22, and Fig. 23.c represented de ductility index according the types concrete. These results consistently highlight the advantages of using UHPFRC in beam-column joints, which can be attributed to the bridging effect of steel fibers, increased tensile strength, and improved ductility observed.

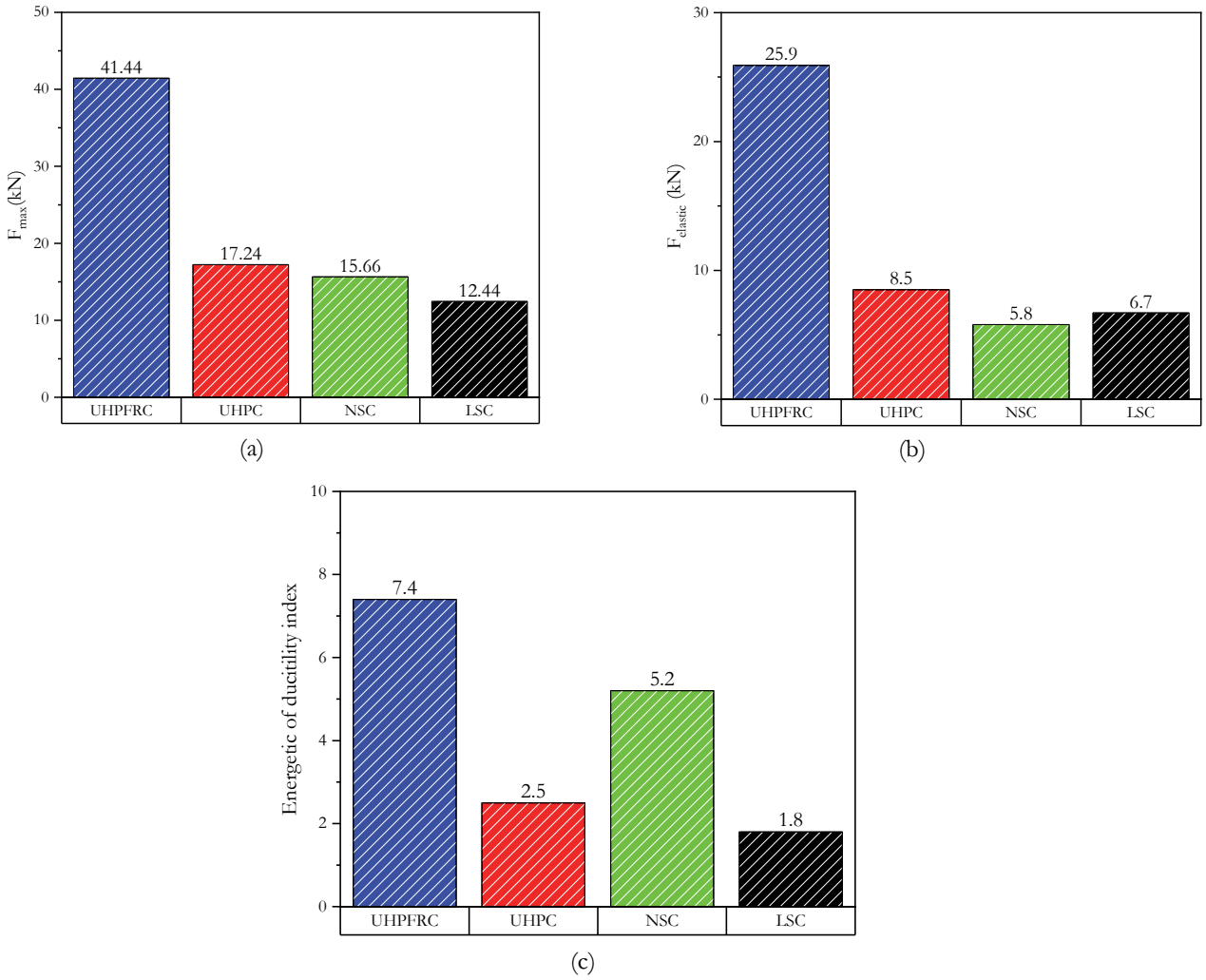

Figure 23: Comparative analysis of (a) strength, (b) elastic force, and (c) energetic ductility index.

The concrete tensile damage index (d_t) is crucial in predicting structural failure. This article analyzes the average damage in various concrete types, as depicted in Fig. 24. These results are obtained by comparing the damage predictions for each finite element within the node region to the total number of finite elements in that region. This methodology enables us to calculate the section's average damage factor. Our analysis reveals a significant value disparity when comparing the utilization of UHPC and UHPFRC. The average damage for NSC and LSC surpasses 70%. Another critical analysis pertains to the damage response compared to the failure mode. NSC experienced failure attributed to the formation of the strut mechanism

in the beam-column joint, whereas, in LSC, rupture predominantly resulted from the development of the strut-and-tie mechanism. This signifies a localized failure concentration within the element, rendering the structure more susceptible to local collapse.

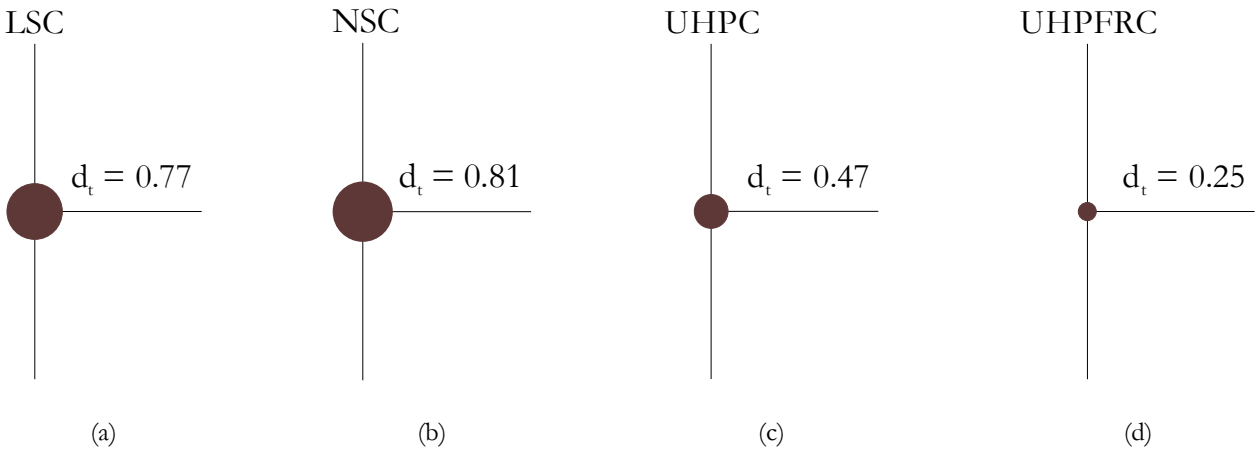

Figure 24: Average damage of tensile: (a) LS, (b) NSC, (c) UHPC, and (d) UHPFRC.

CONCLUSIONS

This paper conducts a comparative analysis of a beam-column joint constructed from LSC, NSC, UHPC, and UHPFRC. Factors such as ultimate strength, damage progression, and ductility behavior are assessed and contrasted. The beam-column joint under examination was experimentally investigated by Cosgun et al. [22], and its numerical model was previously validated by Abdelwahed et al. [23]. Initially, the study validates numerical outcomes from Abaqus against experimental results for LSC. Subsequently, the joint's concrete is replaced to NSC (normal-strength concrete of 25 MPa), UHPC and UHPFRC, both possessing an ultimate resistance of 135 MPa. The main key findings include:

1. The use of UHPFRC in the joint substantially enhances the overall structure's final strength. Compared to LSC, this amplification exceeds 300%, whereas the increase is approximately 250 % for NSC. Additionally, compared to UHPC of equal compressive strength, the joint demonstrates a capacity of 240% superior. This increase can be attributed to the combined contribution of fibers and the matrix.
2. The clear advantage of UHPFRC compared to UHPC is evident, as it presented higher compressive and tensile strength capacity, as supported by the literature [34, 41].
3. The use of UHPFRC results in a ductility index that is 4.11 times that of LSC, 2.96 times that of UHPC, and 1.42 times that of NSC.
4. A notable shift in the failure mechanism of the joint was observed. For LSC and UHPC joints, tensile damage is distributed across the central interface region between the column and beam, forming an inclined tie. In contrast, for UHPFRC, damage is concentrated at the beam's end, with cracks predominantly vertical. This suggests a marked alteration in the joint's failure mode, potentially indicating a need to reassess design criteria.
5. Localized failure concentration within the element signifies that the structure is more susceptible to local collapse. Additionally, NSC and LSC have an average damage that surpasses 70%.

This study aimed to enhance the understanding of the behavior of new high-strength materials, focusing on their capabilities, to be used in joint connections. The ability to accurately predict and effectively evaluate the behavior of these elements can significantly influence the safety and performance of structures specially those subjected to severe lateral loads.

ACKNOWLEDGMENT

This study was financed in part by the Coordenação de Aperfeiçoamento de Pessoal de Nível Superior - Brasil (CAPES) - Finance Code 001, of Conselho Nacional de Desenvolvimento Científico e Tecnológico (CNPq), from Fundação Araucária (FA) and from Financiadora de Estudos e Projetos (FINEP).

REFERENCES

[1] Bosse, R. M. (2022). Curvas de fragilidade e modelos de colapso baseados em dano para pórticos de concreto armado sujeitos à ação sísmica. Universidade de São Paulo.

[2] Bai, J. L., Ou, J. P. (2015). Realization of the global yield mechanism of RC frame structures by redesigning the columns using column tree method. Sci China Technol Sci, 58, 10, pp. 1627–1637, DOI: 10.1007/s11431-015-5875-3.

[3] Ye, L., Qu, Z. (2009). Failure mechanism and its control of building structures under earthquakes based on structural system concept. Journal of Earthquake and Tsunami, 3, 4, pp. 249–259, DOI: 10.1142/S1793431109000627.

[4] Bosse, R. M., Beck, A. T. (2022). Fragility curves and failure models based on lumped damage mechanics applied to reinforced concrete frames under seismic loads. XLII CILAMCE.

[5] Karki, P., Oinam, R. M., Sahoo, D. R. (2020). Evaluation of seismic strengthening techniques for non-ductile soft-story RC frame. Advances in Concrete Construction, 9, 4, pp. 423–435, DOI: 10.12989/acc.2020.9.4.423.

[6] Costa, P. de O. B., Bosse, R. M., Gidrão, G. de M. S. (2022). Behavior assessment of asymmetrical building with concrete damage plasticity (CDP) under seismic load. Frattura ed Integrita Strutturale, 16, 61, pp. 108–118, DOI: 10.3221/IGF-ESIS.61.07.

[7] Taranath, B. S. (2004). Wind and Earthquake Resistant Buildings.

[8] Alva, G. M. S. (2004). Estudo teórico-experimental do comportamento de nós de pórtico de concreto armado submetidos a ações cíclicas. Universidade de São Paulo.

[9] Chetchotisak, P., Arjsri, E., Teerawong, J. (2020). Strut-and-tie model for shear strength prediction of RC exterior beam–column joints under seismic loading. Bulletin of Earthquake Engineering, 18, 4, pp. 1525–1546, DOI: 10.1007/s10518-019-00756-4.

[10] Genesio, G. (2012). Seismic Assessment of RC Exterior Beam-Column Joints and Retrofit with Haunches Using Post-Installed Anchors. Universität Stuttgart.

[11] Haach, V. G. (2005). Análise teórico-experimental da influência da força normal em nós de pórtico externos de concreto armado. Universidade de São Paulo.

[12] Silva, M. (2013). Desenvolvimento de modelo analítico para determinação da resistência ao cisalhamento de nós de pórtico externos de concreto armado. Universidade de São Paulo.

[13] Kim, J., LaFave, J. M. (2007). Key influence parameters for the joint shear behaviour of reinforced concrete (RC) beam-column connections. Eng Struct, 29, 10, pp. 2523–2539, DOI: 10.1016/j.engstruct.2006.12.012.

[14] Yue-Yi, L., Nie, J.G., Ding, R., Fan, J.S. (2023). Seismic performance of squat UHPC shear walls subjected to high-compression shear combined cyclic load. Eng Struct, 276, 115369, DOI: 10.1016/j.engstruct.2022.115369.

[15] Feng, S., Xiao, H., Li, Y. (2022). Influence of interfacial parameters and testing methods on UHPC–NSC bond strength: Slant shear vs. direct tensile testing. Cem Concr Compos, 131, p. 104568, DOI: 10.1016/j.cemconcomp.2022.104568.

[16] Ma, F., Deng, M., Yang, Y. (2021). Experimental study on internal precast beam–column ultra-high-performance concrete connection and shear capacity of its joint. Journal of Building Engineering, 44, p. 103204, DOI: 10.1016/j.jobe.2021.103204.

[17] Xiong, X., Xie, Y., Yao, G., Liu, J., Yan, L., He, L. (2022). Experimental Study on Seismic Performance of Precast Pretensioned Prestressed Concrete Beam-Column Interior Joints Using UHPC for Connection. Materials, 15, 16, DOI: 10.3390/ma15165791.

[18] Zhang, X. , Lu, Y., Wu, X., Wang, P., Li, R., Liu, Y. , Shen C., Zhang H., Zhang D. (2023). Constitutive model for ultra-high performance concrete (UHPC) considering the size effect under cyclic compressive loading. Constr Build Mater, 368, DOI: 10.1016/j.conbuildmat.2023.130499.

[19] Wang, D., Ju, Y., Zheng, W., Shen, H. (2018). Seismic behavior and shear bearing capacity of Ultra-High Performance, Fiber-Reinforced Concrete (UHPFRC) beam-column joints. Applied Sciences (Switzerland), 8, 5, DOI: 10.3390/app8050810.

[20] Cao, Y., Yang, Z. (2022). Seismic Damage Evaluation of Beam-Column Joints in Monolithic Precast Concrete Frame Structures. Materials, 15, 17, DOI: 10.3390/ma15176038.

[21] Zhang, Z. Y., Ding, R., Nie, X., Fan, J. S. (2020). Seismic performance of a novel interior precast concrete beam-column joint using ultra-high performance concrete. Eng Struct, 222, p. 111145, DOI: 10.1016/j.engstruct.2020.111145.

[22] Cosgun, C., Turk, A. M., Mangir, A., Cosgun, T., Kiymaz, G. (2020). Experimental behaviour and failure of beam-column joints with plain bars, low-strength concrete and different anchorage details. Eng Fail Anal, 109, p. 104247, DOI: 10.1016/j.engfailanal.2019.104247.

[23] Abdelwahed, B. S., Kaloop, M. R., El-Demerdash, W. E. (2021). Nonlinear Numerical Assessment of Exterior Beam-Column Connections with Low-Strength Concrete. Buildings, 11, 11, DOI: 10.3390/buildings11110562.
[24] Lubliner, J., Oliver, J., Oller S., Onate, E. (1989). A plastic-damage model for concrete. Int J Solids Struct, 25, 3, pp. 299–326.
[25] Lee, J., Fenves, G. L. (1998). Plastic-Damage Model for Cyclic Loading of Concrete Structures. J Eng Mech, 124, 8, pp. 892–900, DOI: 10.1061/(asce)0733-9399(1998)124:8(892).
[26] Xiao, Y., Chen, Z., Zhou, J., Leng, Y., Xia, R. (2017). Concrete plastic-damage factor for finite element analysis: Concept, simulation, and experiment. Advances in Mechanical Engineering, 9, 9, pp. 1–10, DOI: 10.1177/1687814017719642.
[27] Le Minh, H., Khatir, S., Abdelwahab, M., Cuong-Le, T. (2021). A concrete damage plasticity model for predicting the effects of compressive high-strength concrete under static and dynamic loads. Journal of Building Engineering, 44, March, p. 103239, DOI: 10.1016/j.jobe.2021.103239.
[28] Grassl, P., Xenos, D., Ulrika, N., Rempling, R., Gylltoft, K. (2013). CDPM2: A damage-plasticity approach to modelling the failure of concrete.pdf. Int J Solids Struct.
[29] Kakavand, M. R. A., Taciroglu, E. (2020). An enhanced damage plasticity model for predicting the cyclic behavior of plain concrete under multiaxial loading conditions. Frontiers of Structural and Civil Engineering, 14, 6, pp. 1531–1544, DOI: 10.1007/s11709-020-0675-7.
[30] Genikomsou, A. S., Polak, M. A. (2015). Finite element analysis of punching shear of concrete slabs using damaged plasticity model in ABAQUS. Eng Struct, 98, pp. 38–48, DOI: 10.1016/j.engstruct.2015.04.016.
[31] Grassl, P., Jirásek, M. (2006). Damage-plastic model for concrete failure. Int J Solids Struct, 43, 22–23, pp. 7166–7196, DOI: 10.1016/j.ijsolstr.2006.06.032.
[32] Leimatre, J., Chaboche, J.L. (1994). Mechanics of solid materials.
[33] Alejano L. R., Bobet A. (2012). Drucker-Prager criterion. Rock Mech Rock Eng, 45, 6, pp. 995–999, DOI: 10.1007/s00603-012-0278-2.
[34] Gidrão G. de M. S. (2020). Estudo numérico e experimental do comportamento cíclico de vigas I protendidas de concreto de altíssimo desempenho. Universidade de São Paulo.
[35] Abaqus (2014). ABAQUS/CAE User's Manual, Version 6.14. Dassault Systèmes.
[36] Krahl P.A., Carrazedo R., El-Debs M. K. (2018). Mechanical damage evolution in UHPFRC: Experimental and numerical investigation. Eng Struct, 170, DOI: 10.1016/j.engstruct.2018.05.064.
[37] Callister, W. D., Rethwish, D. G. (2016). Ciência e engenharia de materiais: uma introdução, 9th ed.
[38] Naaman, A. E. (2003). FRP Reinforcements in Structural Concrete: Assessment, Progress and Prospects. Fibre-Reinforced Polymer Reinforcement for Concrete Structures, pp. 3–24, DOI: 10.1142/9789812704863_0001.
[39] Machado, M. G. (2004). Estudo Experimental da Ductilidade de Vigas em Concreto Armado Reforçadas à Flexão Utilizando Compósitos com Tecido de Fibras de CarboPontifícia Universidade Católica do Rio de Janeiro.
[40] El Zareef, M. A., El Madawy, M. E. (2018). Effect of glass-fiber rods on the ductile behaviour of reinforced concrete beams. Alexandria Engineering Journal, 57, 4, pp. 4071–4079, 2018, DOI: 10.1016/j.aej.2018.03.012.
[41] AFGC (2013). Ultra High Performance Fibre-Reinforced Concretes Recommendations.
[42] AFNOR (2016). NF P 18-710 - National addition to Eurocode 2 — Design of concrete structures: specific rules for Ultra-
[43] Ahmad, S., Pilakoutas, K., Khan, Q. Z., Neocleous, K. (2015). Stress–Strain Model for Low-Strength Concrete in Uni-Axial Compression. Arab J Sci Eng, 40, 2, pp. 313–328, DOI: 10.1007/s13369-014-1411-1.
[44] ACI 318 (2019). Building Code Requirements for Structural Concrete and Commentary.
[45] Eurocode (2004). Eurocode 2: Design of concrete structures - Part 1-1 : General rules and rules for buildings Eurocode.
[46] CEB FIP Model Code (2010). First complete draft - 1.
[47] Kumar, P. (2004). A compact analytical material model for unconfined concrete under uni-axial compression. Materials and Structures/Materiaux et Constructions, 37, 273, pp. 585–590, DOI: 10.1617/13974.
[48] Sima, J. F., Roca, P., Molins, C. (2008). Cyclic constitutive model for concrete. Eng Struct, 30, 3, pp. 695–706, DOI: 10.1016/j.engstruct.2007.05.005.
[49] Carreira, D. J., Chu, K. (1985). Stress-Strain Relatonship for Reinforced Concrete in Compression. ACI Struct J, November-December, pp. 797–804.
[50] ABNT (2023). NBR 6118 - Projeto de estruturas de concreto. Associação Brasileira de Normas Técnicas.
[51] Singh, K., Saini, J. S., Bhunia, H. (2017). Effect of metallic inserts on the strength of pin joints prepared from glass fiber reinforced composites. Def Sci J, 67, 5, pp. 592–600, DOI: 10.14429/dsj.67.11041.

[52] Shi, K., Zhang, M., Zhang, T., Xue, R., Li, P. (2021). Analysis on the seismic performance of steel fiber-reinforced high-strength concrete beam–column joints. Materials, 14, 14, DOI: 10.3390/ma14144016.

[53] Yu, F., Zou, Q., Fang, Y., Li, D., Bu, S. (2022). Deformation analysis of axially loaded weak PVC-fiber reinforced polymer confined concrete column-strong reinforced concrete beam joints reinforced with core steel tube. Advances in Structural Engineering, 25, 3, pp. 642–661, DOI: 10.1177/13694332211064662.